PAPER

Can heteroatom and heteroarene annelations make pentalenes suitable as singlet fission chromophores?

Emil Säbb, [ID] Péter J. Mayer [ID] and Henrik Ottosson [ID] *

Pentalene derivatives were previously hypothesised to have potential as singlet fission (SF) chromophores, but their function is hampered by both the symmetry-forbidden transition to the first singlet excited state (S_1) and the thermal instability due to antiaromatic character in their ground state (S_0). A possible benefit is Baird-aromatic character in the lowest $\pi\pi^*$ excited states, which may confer higher photochemical stability compared to current SF chromophores. In this computational work, we explored different heteroatomic replacements on the pentalene skeleton as well as heteroareno fusions with the aim to identify derivatives with (i) allowed transitions to S_1, (ii) reduced antiaromatic character in S_0, (iii) highly Baird-aromatic pentalene cores in T_1 and S_1, and (iv) the SF energy criteria ($2 \leq E(S_1)/E(T_1)$ and $E(S_1) < E(T_2)$) fulfilled. The results show that the symmetry-forbidden nature of the transition to S_1 can be alleviated, while maintaining excited state Baird-aromatic character conferring photostability. However, there are other drawbacks that impede the use of pentalenes as SF chromophores: (i) the $E(S_1)/E(T_1)$ ratios when adiabatic S_1 states are considered are in nearly all cases well below 2 as the pentalene cores exhibit large relaxation energies in this state (thus both adiabatic $E(S_1)$ and $E(T_1)$ must be used for Baird-aromatic SF chromophore candidates), and (ii) competing decay pathways exist due to accessible S_1/S_0 conical intersections. Hence, the design of pentalene derivatives that are suitable as SF chromophores will be challenging. Still, our findings may pave the way to other related species for which all drawbacks can be avoided.

Introduction

Pentalene and its derivatives are an interesting class of organic molecules for many reasons, one being the excited-state aromatic character of the 8π-electron pentalene core.[1–8] However, a drawback for their use in optical devices is the symmetry-forbidden transition from the ground state (S_0) to the first excited singlet state (S_1), as this prevents the direct excitation into the state that normally influences the subsequent photophysics and photochemistry.[9] This may particularly hamper the potential application of pentalenes as singlet fission (SF) chromophores, *i.e.*, light-absorbing molecules which after excitation are able to undergo a spin-allowed process in which a chromophore molecule in S_1 and another chromophore molecule in the S_0 state form two free triplet state (T_1) chromophores through a spin-allowed fission process.[10] This charge carrier multiplication process can benefit future solar energy harvesting applications by allowing photovoltaic cells to overcome the theoretical Shockley–Queisser limit of 33% for single-junction

solar cells.[11] We earlier postulated that pentalenes could be useful as SF chromophores,[12] but this needs to be evaluated further. In this context, gradually more efforts have been devoted to the synthesis and subsequent experimental studies of various heteroarenopentalenes[3,13,14] and heteropentalenes.[15–20] Research has also been carried out on the impact of annelations on the photophysics of heteroarenopentalenes.[18]

We used quantum chemical computations to explore a series of mono(heteroareno)pentalenes (Fig. 1), analogous to monobenzopentalene (**MBP**), as well as carbon-to-heteroatom replacements on the pentalene core to address the problem of the symmetry-forbidden lowest transition of pentalenes related to their potential application in SF photovoltaics. Focus was placed on increased oscillator strengths for the transition to S_1, *i.e.*, $f(S_0–S_1)$. The structural modifications were first performed with replacement of the benzene ring of **MBP** by a single heteroarene ring having one heteroatom (class A, Fig. 1) to evaluate if the replacement pattern impacts $f(S_0–S_1)$ and the S_1 and T_1 state energies ($E(S_1)$ and $E(T_1)$), followed by replacement of the benzene ring by heteroarenes with two heteroatoms (class B, Fig. 1). This was expanded by heteroatomic replacements on the pentalene core (class C, Fig. 1). Finally, we

Department of Chemistry –Ångström, Uppsala University, Box 523, Uppsala 751 20, Sweden. E-mail: henrik.ottosson@kemi.uu.se
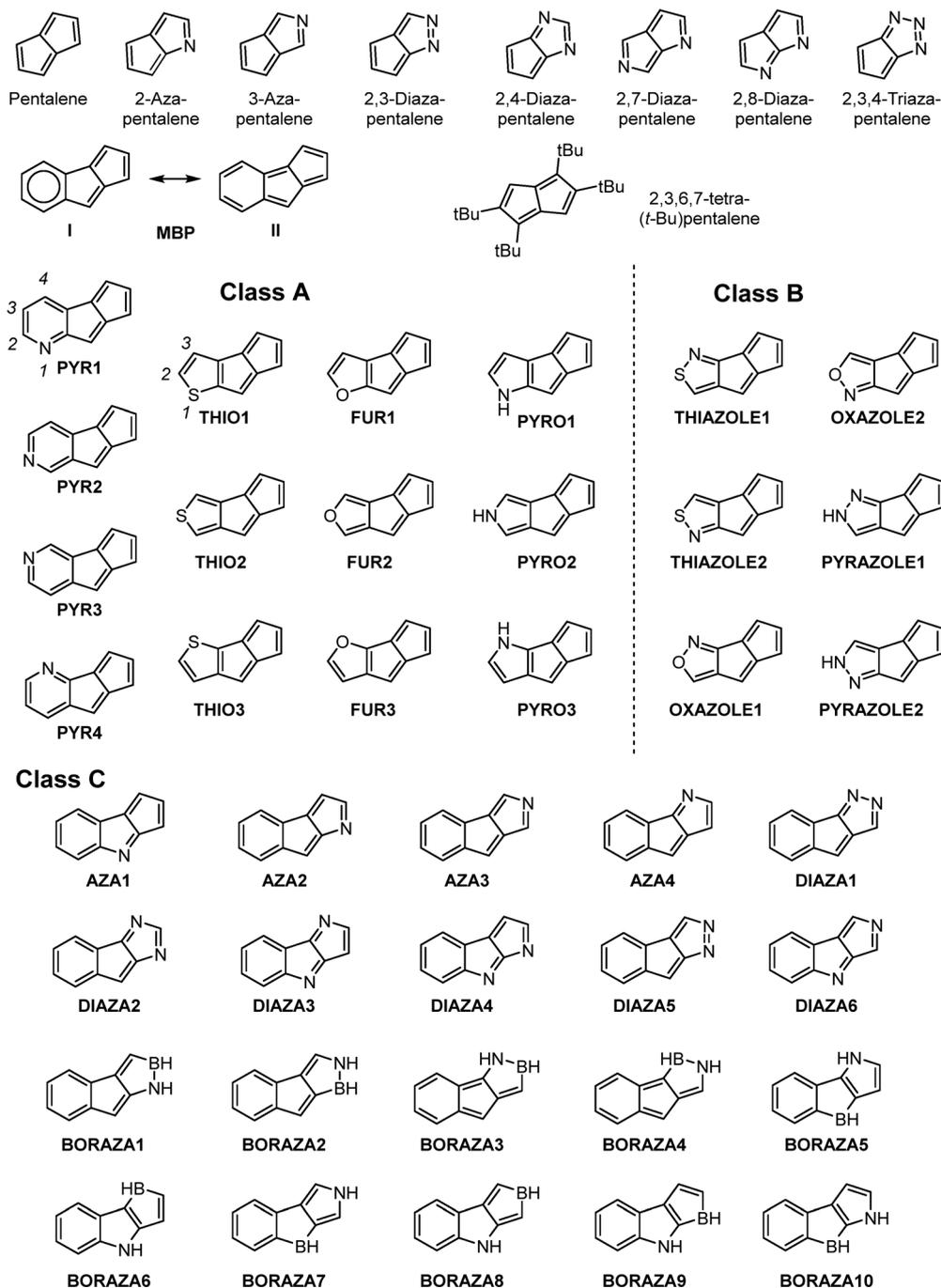
Fig. 1 Pentalene, mono-, di-, and triazapentalenes, tetra(*tert*-butyl)pentalene, monobenzopentalene (**MBP**), and the investigated heteroatom substituted arenopentalenes grouped into three classes: mono(heteroareno)pentalenes with one heteroatom (class A), mono(heteroareno)pentalenes with two heteroatoms (class B), and benzoheteropentalenes (class C).

combined the best-performing modifications in classes A–C into a few bis(heteroareno)pentalenes (class D, *vide infra*). Throughout our investigation, we compare the computed $f(S_0–S_1)$ values to those of a set of well-established SF chromophores (tetracene, pentacene and 1,3-diphenylisobenzofuran).

In addition to the analysis of the change in $f(S_0–S_1)$, we evaluated the T_1 state Baird-aromatic character of the pentalene derivatives in their 8π-electron cores as approximates of the

aromatic character in their lowest $\pi\pi^*$ states (both T_1 and S_1). Such aromatic character can increase their photochemical stability,[12,21–25] even though it may instead lead to lowered kinetic stability of the excited states as a result of smaller energy gaps between S_1 and S_0 (*vide infra*). To estimate their thermal stabilities, we compared their computed antiaromatic character in S_0 to those of two pentalene derivatives that are known to be persistent at ambient temperature: 1,3,5-tri(*tert*-butyl)pentalene

This journal is © the Owner Societies 2026

Phys. Chem. Chem. Phys., 2026, **28**, 6894–6907 | **6895**

and dibenzo[*a,e*]pentalene.[26,27] The stability of the first is achieved by the three bulky groups, and thus its pentalene core is still strongly antiaromatic in S_0. The second pentalene, on the other hand, has attenuated antiaromatic character[28] and may be viewed as two interconnected styrene molecules.

A number of SF chromophores are known, *e.g.*, acenes, isobenzofurans, and diphenyl-hexatrienes,[29] as well as one dibenzopentalene derivative, 1,8-bis(styryl)dibenzopentalene.[30] In the last compound, the spin density of the T_1 state is, however, mostly centred on 1,8-diphenyloctatetraene and not on the pentalene moiety.[12] In S_0, these molecules often have formally aromatic moieties, but they either have an attenuated aromaticity or have no aromatic character in this state. At the same time, it is known that aromatic character in the lowest $\pi\pi^*$ excited state may provide a means for designing new SF chromophores.[12] Aromaticity in $\pi\pi^*$ excited states often follows different electron counting rules compared to the π-electron counting rules for the S_0 state, *i.e.*, Hückel's rule. This means that $4n\pi$-electron species can be aromatic in their lowest $\pi\pi^*$ states, while those with $4n + 2$ π-electrons are antiaromatic, a rule known as Baird's rule.[31–36]

Indeed, molecules with antiaromatic S_0 states generally have aromatic lowest excited $\pi\pi^*$ states, and therefore they usually have a lower energy between S_0 and S_1 than nonaromatic isomers.[12,32,37,38] This relationship between ground- and excited-state (anti)aromatic character and excitation energy means that tuning the degree of (anti)aromaticity allows for energy tuning of the S_1 and T_1 states relative to the S_0 state,[12,39] provided the S_1 and T_1 states are described by the same electron configuration (except for its multiplicity). For substituted fulvenes (especially protonated dicyanofulvenes), it is even possible to tune the relative energies of the lowest singlet and triplet states gradually until the Baird-aromatic triplet state becomes the electronic ground state dominated by a resonance structure with a cyclopentadienyl cationic ring (Fig. 2).[40] Noteworthily, both the parent cyclopentadienyl cation and the pentachloro substituted derivative, representing the extreme point of triplet state Baird-aromatic fulvenes, are known from EPR spectroscopy experiments to have triplet ground states.[41,42] In theory, it should thus be possible to achieve compounds that fulfil the first SF criterion $2E(T_1) < E(S_1)$ in the region to the right in Fig. 2.

As noted above, the influence of excited state aromatic character can lead to higher photochemical stability against detrimental side reactions.[32,38] Additionally, we recently found in computations that compounds with strongly Baird-aromatic T_1 states have very low spin–orbit coupling (SOC) between their T_1 and S_0 states.[43] This may lead to long-lived triplet states, which could be beneficial for the diffusion of the triplet exciton in a thin film of the SF chromophore.[10,44]

One of the compound classes that were previously suggested as potential SF chromophores was **MBP** derivatives.[12] In another recent work, it was shown that the synthetically available family of **MBP**s can overcome the shortcoming of a low-lying T_2 state of the pentalene core.[45] However, even though substituted **MBP**s on paper may have the possibility to exhibit SF, no proof of this has been shown, and the lack of SF was hypothesized to originate from the dark character of the S_1
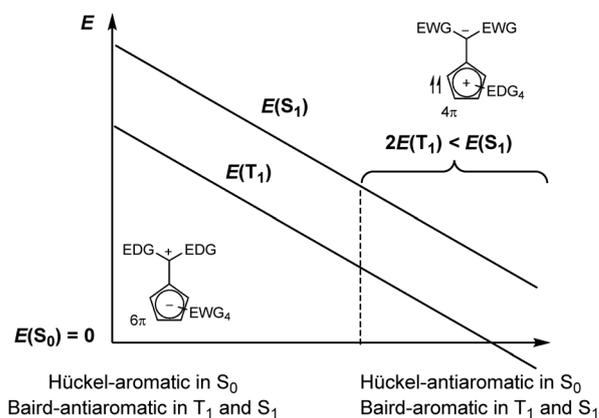

Fig. 2 A schematic diagram showing how the S_1 and T_1 energies of substituted fulvenes vary as a function of Hückel-aromatic/antiaromatic character in the S_0 state and Baird-antiaromatic/aromatic character in the T_1 and S_1 states. EDG = electron-donating group and EWG = electron-withdrawing group.

state. Excitations to higher singlet states yielded only weak anti-Kasha emission and no emission from S_1.[45] It was also noticed that the substituents along **MBP**'s perimeter had little to no effect on $f(S_0–S_1)$.[45]

The symmetry-forbidden character of the S_0-to-S_1 transition of the parent pentalene, described by a singly excited HOMO → LUMO configuration, is analogous to those of other planar Hückel-antiaromatic $4n\pi$-electron all-carbon molecules, where the direct excitation to S_1 has a symmetry-forbidden $\pi\pi^*$ character.[9] Thus, and as earlier argued,[19,46] alleviation of S_0 antiaromaticity, which attenuates the thermal instability, may simultaneously alleviate the symmetry-forbidden character for this transition. Indeed, carbon-to-heteroatom replacements have previously been used to increase $f(S_0–S_1)$ in other $4n\pi$-electron species while also achieving detectable emission from the S_1 state.[37–39] Together, these features may render pentalene derivatives interesting as SF chromophores.

Still, there is a caveat with pentalenes as SF chromophores, not addressed earlier in studies on their potential SF applications, as the parent pentalene has a readily available conical intersection (CI) leading from the S_1 to the S_0 state.[47] This feature provides an excited pentalene with a fast relaxation pathway to S_0, and if it remains in the benzannelated derivatives (see Section S6 in the SI), this will severely hamper the use of such pentalenes as SF chromophores. This could, in part, explain why **MBP** has a non-emissive S_1 state.[45] Yet, even in the absence of a CI, the small energy gap between the S_1 and S_0 states at the optimised S_1 state geometries of benzannelated pentalenes may promote radiationless hopping from the S_1 to the S_0 surface. Such jumps are probable in all-carbon $4n\pi$-electron species known to exhibit fast radiationless decay.[48] Even though the computation of the activation barrier to the CI geometry for all of the compounds is outside the scope of this study, the energy gap between S_1 and S_0 states was evaluated using CASSCF computations for a few selected compounds.

Taken together, we use computations to scrutinize the potential of pentalene derivatives as SF chromophore candidates from a

6896 | *Phys. Chem. Chem. Phys.*, 2026, **28**, 6894–6907

This journal is © the Owner Societies 2026

number of perspectives. The ambition is to facilitate the search for such compounds based on pentalene or, alternatively, based on compounds that in some ways are related to pentalenes. A wider objective is to identify caveats of compounds that are (strongly) Baird-aromatic in their T_1 and S_1 states when explored as tentative SF chromophore candidates.

Results and discussion

After a brief description of the computational tools used in the study, we present results on $f(S_0-S_1)$, which reveal to what extent these values can be increased to reach values that are representative of current SF chromophores, followed by a discussion of the $E(S_1)/E(T_1)$ ratios used to predict if a pentalene derivative can be suitable as an SF chromophore. Yet, we further explore features on the S_1 surface that can jeopardize the use of pentalenes for singlet fission, and, more explicitly, if there are conical intersections near the minimum on the S_1 PES. Finally, we utilize the knowledge gained from the results of the compounds in groups A–C to the design of bis(heteroareno)pentalenes and (heteroareno)heteropentalenes, where we seek to maximise $f(S_0-S_1)$ and the $E(S_1)/E(T_1)$ ratio toward what is relevant for SF, while maintaining (moderately) Baird-aromatic character in T_1. Noteworthily, the second SF criterion ($E(S_1) < E(T_2)$) is satisfied for all our investigated pentalene derivatives, with the vertical T_2 state typically $\sim$1 eV above the vertical S_1 state (see Table S1). Thus, this criterion is not discussed further herein. It should also be noted that the T_1 and S_1 states are of $\pi\pi^*$ character in essentially all compounds, the exception being **DIAZA5** with an $n\pi^*$ state as the lowest excited state.

Computational tools

The M06-2X functional was chosen based on earlier computational work that showed good agreement for the calculated energy orderings of the S_1, T_1 and S_0 states of pentalenes when compared to CASPT2 results.[12] To optimize the S_1 state geometries of the heteroarenopentalenes, which failed to converge under linear TD-DFT geometry optimisations, we used spin-flip-TD-DFT (SF-TD-DFT). This is a computational method used to interpret multiconfigurational wavefunctions in terms of single-reference formalism.[49] However, this method is susceptible to spin contamination (*i.e.*, impure spin states) if the states involved have a large contribution from double excitations to configurations with doubly-occupied virtual orbitals, leading to unreliable results.[49] To assess the quality of these optimized geometries, a subset of molecules was also investigated through geometry optimisation at the multireference CASSCF level, with energies and orbital occupancies at the CASPT2 level, which includes second-order perturbation theory corrections. For further details and references, see the Computational methodology section.

In the second part of the study, we applied various computational descriptors that assess the extent of aromatic or antiaromatic character (abbr. (anti)aromatic) of a cyclic molecule or a segment of a polycyclic molecule.[50] The pentalene derivatives were analysed using descriptors that represent the electronic,

magnetic and geometric aspects of (anti)aromaticity (the energetic was not considered). For the electronic aspect, we used the multicenter index (MCI)[51] and the fluctuation index (FLU),[52–54] which give information on the extent of electron delocalization throughout a cycle. More specifically, FLU explores the fluctuation in the π-electron sharing between neighbouring atoms in a cycle, while MCI investigates the electron sharing between all atomic pairs in a cycle. The magnetic aspect was analysed *via* both the anisotropy of the induced current density (AICD, or more often ACID)[55,56] as well as the nucleus independent chemical shift (NICS)[57–62] as a probe of magnetically induced ring currents. Thirdly, the harmonic oscillator model of aromaticity (HOMA)[63,64] was applied as a geometric descriptor to evaluate to what extent bond length equalization reveals aromaticity.

Now, what values do the descriptors adopt when representing, respectively, aromaticity and antiaromaticity? With MCI, the values that represent aromaticity are as high as possible approaching the value of a known aromatic reference compound of the same ring size, while the FLU values of aromatic cycles approach zero. Yet, neither of these electronic indices can distinguish between antiaromatic and nonaromatic cycles, which in contrast is possible with magnetic descriptors. Aromatic cycles exhibit diatropic ring currents (shown as clockwise in our ACID plots), *i.e.*, induced ring currents that counteract the applied magnetic field, while antiaromatic cycles show paratropic (counter-clockwise) ring currents that instead enhance the magnetic field. NICS values are the negative of the shielding at a chosen point in space, and indicate aromatic character if clearly negative (<-5 ppm), antiaromatic character if positive (>5 ppm), and values close to zero suggest nonaromatic character. Yet, the NICS descriptor has pitfalls because negative (positive) NICS values do not necessarily result from diatropic (paratropic) ring currents in a particular ring.[65] Instead, they can result from a ring current of opposite tropicity in an adjacent ring in a polycyclic molecule or from local circulations in the current density, *e.g.*, at heteroatoms. Finally, HOMA values in the range of 0.5–1.0 indicate aromaticity, while those below represent nonaromatic or antiaromatic character. For proper (anti)aromaticity assessments, it is crucial to know the limitations of the various descriptors.

Oscillator strengths

The $f(S_0-S_1)$ values of class A pentalenes are the largest in **PYR3**, **THIO2**, **FUR2**, and **PYRO1** (Table 1, entries 13, 16, 19, and 21, respectively), with values up to ten times larger than that in **MBP** (Table 1, entry 10). Yet, when compared to the correspondingly computed oscillator strengths of tetracene, pentacene and 1,3-diphenylisobenzofuran as established SF chromophores ($f(S_0-S_1)$ = 0.0620, 0.0394 and 0.5007, respectively), we see that the values of the best class A pentalenes are only modest.

A general trend was observed for pentalenes annelated with 5-membered ring (5-MR) heteroaromatics: the smallest $f(S_0-S_1)$ values, as shown in Table 1, entries 15–23, were computed for structures with the heteroatom in the position labelled 3 in Fig. 1, intermediate values were observed with the heteroatom in position 1, and the highest $f(S_1-S_0)$ values are observed with heteroatoms in position 2 (except for **PYRO2**). As the antiaromatic

This journal is © the Owner Societies 2026

Phys. Chem. Chem. Phys., 2026, **28**, 6894–6907 | **6897**

Table 1 Calculated $f(S_0-S_1)$ and energies of the S_1 and T_1 states for all molecules in Fig. 1

Entry	Molecule	$f(S_0-S_1)$	$E(T_{1a})$ (eV)	$E(S_{1v})$ (eV)	$E(S_{1v})/E(T_{1a})$
1	**Pentalene**	0	0.63	1.92	3.06
2	**2-Azapentalene**	0.0013	0.62	2.16	3.50
3	**3-Azapentalene**	0.0010	0.87	2.10	2.42
4	**2,3-Diazapentalene**	0.0014	0.86	2.40	2.79
5	**2,4-Diazapentalene**	Triplet ground state			
6	**2,7-Diazapentalene**	0.0060	0.76	2.44	3.20
7	**2,8-Diazapentalene**	Triplet ground state			
8	**2,3,4-Triazapentalene**	0.0015	0.79	2.58	3.24
9	**2,3,6,7-Tetra(_t_-Bu)pentalene**	0	0.55	1.83	3.33
10	**Monobenzopentalene (MBP)**	0.0008	1.06	2.32	2.18
11	**PYR1**	0.0011	1.05	2.37	2.26
12	**PYR2**	0.0013	1.11	2.40	2.16
13	**PYR3**	0.0041	1.01	2.37	2.35
14	**PYR4**	0.0004	1.07	2.35	2.19
15	**THIO1**	0.0018	0.75	1.92	2.55
16	**THIO2**	0.0026	1.16	2.52	2.18
17	**THIO3**	0.0005	0.75	1.89	2.50
18	**FUR1**	0.0058	0.63	1.81	2.88
19	**FUR2**	0.0078	1.19	2.70	2.26
20	**FUR3**	0.0007	0.65	1.75	2.68
21	**PYRO1**	0.0052	0.68	1.79	2.64
22	**PYRO2**	0.0034	1.09	2.43	2.22
23	**PYRO3**	0.0002	0.72	1.74	2.41
24	**THIAZOLE1**	0.0029	1.18	2.51	2.13
25	**THIAZOLE2**	0.0018	1.12	2.51	2.23
26	**OXAZOLE1**	0.0074	1.26	2.76	2.19
27	**OXAZOLE2**	0.0069	1.15	2.67	2.32
28	**PYRAZOLE1**	0.0043	1.12	2.43	2.17
29	**PYRAZOLE2**	0.0025	1.18	2.43	2.29
30	**AZA1**	0.0029	0.93	2.30	2.47
31	**AZA2**	0.0018	1.15	2.52	2.18
32	**AZA3**	0.0014	1.12	2.50	2.23
33	**AZA4**	0.0027	0.90	2.34	2.60
34	**DIAZA1**	0.0024	1.22	2.68	2.20
35	**DIAZA2**	0.0057	1.00	2.47	2.48
36	**DIAZA3**	0.0006	0.86	2.35	2.73
37	**DIAZA4**	0.0011	1.12	2.53	2.26
38	**DIAZA5**	0.0011	1.06	2.37	2.24
39	**DIAZA6**	0.0052	1.01	2.49	2.46
40	**BORAZA1**	0.0076	1.50	2.78	1.86
41	**BORAZA2**	0.0263	1.64	2.92	1.78
42	**BORAZA3**	Triplet ground state			
43	**BORAZA4**	0.0099	0.53	1.52	2.85
44	**BORAZA5**	0.0048	1.91	2.84	1.49
45	**BORAZA6**	0.0033	1.12	2.30	2.05
46	**BORAZA7**	0.0034	2.48	3.35	1.35
47	**BORAZA8**	0.0036	0.78	1.89	2.42
48	**BORAZA9**	0.0024	0.87	1.93	2.22
49	**BORAZA10**	0.0073	1.82	2.77	1.52

character in S_0 is almost the same for molecules with a heteroatom in position 1 or 3 (_vide infra_), leading to similar annellation patterns,[28] our finding indicates that factors beyond (anti)aromaticity impact the allowedness of the transition. One may argue that the difference in permanent dipole moment between the two types of structures has an influence, but a lack of correlation between $f(S_0-S_1)$ and dipole moment disputes this argument (Fig. S49).

The non-zero oscillator strength is found to originate from the spatial dissymmetry and displacement of the orbitals involved in the HOMO → LUMO transition. As shown in Fig. 3, the orbitals change from a transition between the symmetrical HOMO and LUMO in pentalene ($f(S_0-S_1) = 0$) to an intermediate case in

PYRO1, having an extended HOMO but a pentalene-centered LUMO (Fig. 3B), and to a significantly distorted HOMO and an increased distortion also of the LUMO in **FUR2** (Fig. 3C). The same general features hold true when comparing to **MBP** (Fig. 3D), with more similarities between **PYRO1** and **MBP**. This change in the spatial distribution of the two MOs makes the S_0–S_1 transition more accessible. However, if the spatial displacement is too extensive, it will lead to a transition with large charge-transfer character, and accordingly, a small S_1–T_1 energy splitting similar to that in azulene, in which the HOMO is localised on 5-MR and the LUMO on 7-MR.[66] Yet, the spatial separation between the HOMO and the LUMO can also involve localisation of the two orbitals on different sets of atoms within the same cyclic path, and this occurs in pentalene at its relaxed D_{2h} symmetric geometries in the S_1 and T_1 states.[16]

Based on the shift in electron density in the pentalene derivatives upon HOMO → LUMO excitations, one may anticipate the permanent dipole moments to change. Indeed, the dipole moment in the T_1 states of many of the pentalenes increase when compared to those in S_0, in a few by up to 0.9 D, but mostly by less than 0.5 D (Fig. S50). As the S_1 states are described by the same electron configuration (except for multiplicity), this suggests that solvent polarity can have an effect on the transitions and potentially also lead to some solvatochromism.

By moving to classes B and C, we explore the effect of further carbon-to-heteroatom replacements _via_ (i) pyrazolo-, isoxazolo-, and isothiazolo-annelated pentalenes (class B) and (ii) carbon-to-heteroatom replacements in the pentalene core of a mono-benzopentalene (class C). The annelation pattern chosen for the class B pentalenes was the pattern among the class A pentalenes that led to the highest increase in $f(S_0-S_1)$ compared to the value of **MBP**. However, the results indicate that $f(S_0-S_1)$ is comparable to those of their annelated analogues in class A (Table 1, entries 16, 19, 22 and 24–29). This type of replacement pattern was therefore not further investigated. Our focus instead turned to heteroatom replacements in the pentalene core, _i.e._, class C compounds (Fig. 1). Such pentalenes have received recent attention,[13] and in those studies it was observed that substituents at the pentalene can have large effects on the energies of the lowest excited states. Nevertheless, the substituent effects on $f(S_0-S_1)$ were minimal.[18,38,45]

The two parent monoazapentalenes, 2- and 3-azapentalene, have nonzero but still minute $f(S_0-S_1)$, although they may work as templates for further modifications on the pentalene core (Table 1, entries 2 and 3). For the diaza- and triazapentalenes, it was found that 2,7-diazapentalene exhibited a uniquely high $f(S_0-S_1)$ value (Table 1, entries 4–7), while most others showed lower values. Noteworthily, two diazapentalenes were computed to have triplet ground states (T_0) (Table 1, entries 5 and 7), which makes them impossible as SF chromophores.

Among class C compounds, the replacement of just one C atom with one N in the pentalene core (**AZA1–AZA4**) (Table 1, entries 30–33) had a small effect on the calculated $f(S_0-S_1)$ when compared to **MBP** (at most a factor 3 increase). This was also the case when two C atoms were replaced symmetrically with two N atoms (**DIAZA3**, Table 1, entry 36), in line with
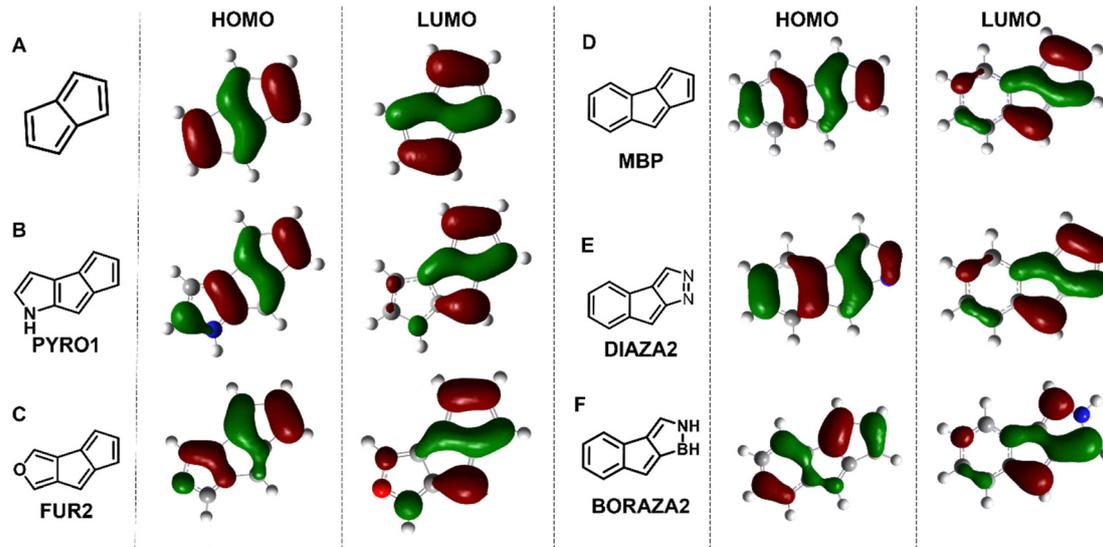
6898 | _Phys. Chem. Chem. Phys._, 2026, **28**, 6894–6907

This journal is © the Owner Societies 2026

Fig. 3 The calculated HOMOs and LUMOs of (A) pentalene, (B) **PYRO1**, (C) **FUR2**, (D) **MBP**, (E) **DIAZA2** and (F) **BORAZA2**. The frontier molecular orbitals are visualized at a 0.04 isosurface value.

experimental observations.[19] However, larger $f(S_0–S_1)$ values resulted when the two N atoms were placed unsymmetrically. Particularly, **DIAZA2** and **DIAZA6** exhibited large $f(S_0–S_1)$ values with an 8-fold increase for **DIAZA2** when compared to **MBP** (Table 1, entries 35 and 39), explained by the distortion of the HOMO of **DIAZA2** (Fig. 3E). Thus, certain annelated diazapentalenes exhibit notable increases in their $f(S_0–S_1)$ values, also when compared to the corresponding parent diazapentalenes (Table 1, entries 4–7). The increase in $f(S_0–S_1)$ is, however, insufficient to reach the values of pentacene, tetracene and 1,3-diphenyl-isobenzofurane, which are 8–100 times higher than that of **DIAZA2**.

For the C$_2$-to-BN replacements in the pentalene core of **MBP**, giving the boraza-derivatives in class C, we did not consider replacements that lead to mesoionic isomers, i.e., species that must be described with zwitterionic resonance structures.[67] For the boraza-analogues of cyclooctatetraene, it was shown previously that the mesoionic character destabilizes the S$_0$ state extensively,[68] and thus one can argue that a mesoionic borazapentalene will be less thermally stable than pentalene. Due to the destabilization of S$_0$, such a borazapentalene would also have a small $E(T_1)$, whereby it is unlikely to have an electronically extractable T$_1$ state in conjunction with silicon solar cells.

The single C$_2$-to-BN replacement to regular monobenzoborazapentalenes had the largest effect on $f(S_0–S_1)$ when the B and N atoms were on the opposite side of the pentalene core relative to the benzene ring, as in **BORAZA2** and **BORAZA4** (Table 1, entries 41 and 43). Among these compounds, **BORAZA2** had the largest oscillator strength (0.0263), being 33 times higher than that of **MBP** and approaching that of pentacene (0.0394). However, as is clear from the HOMO and LUMO of **BORAZA2** (Fig. 3F), the monobenzoborazapentalenes have frontier orbitals which are dissimilar from those of parent pentalene and

MBP. Thus, to call them pentalene derivatives is, in our view, misleading in a strict electronic structural sense.

$E(S_1)/E(T_1)$ ratios

Next, we explored for the molecules in classes A–C to what extent the first of the two SF energy criteria is satisfied, i.e., $2 \leq E(S_1)/E(T_1)$. An initial estimation of the SF capabilities of the various compounds was based on the adiabatic T$_1$ ($E(T_{1a})$) and vertical S$_1$ energies ($E(S_{1v})$) following the approach by Zeng, Hoffmann and Ananth (ZHA).[69] However, this approach is susceptible to overestimation of the $E(S_1)/E(T_1)$ ratios, and we observed that it is unsuitable for molecules that are Baird-aromatic in S$_1$. According to the ZHA approach, all structures in classes A–C, except for a few of the **BORAZA** compounds, satisfy the SF criterion $2 < E(S_{1v})/E(T_{1a})$ (Table 1, entries 10–39). Yet, when the S$_1$ state is relaxed, the molecules often undergo extensive geometry changes as they relax from the vertically excited S$_0$ structure. The S$_0$ structure has a bond length alternate pentalene moiety (formally Hückel-antiaromatic in S$_0$) and a weakly Hückel-aromatic benzene ring (Fig. 4). In the excited
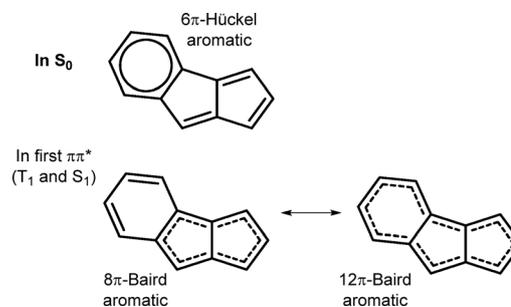

Fig. 4 Illustration of how **MBP** can be influenced by the 6π-electron Hückel-aromatic character in S$_0$ and 8π- and 12π-electron Baird-aromatic character in T$_1$ and S$_1$.

This journal is © the Owner Societies 2026

Phys. Chem. Chem. Phys., 2026, **28**, 6894–6907 | **6899**

state, this relaxes to a structure which is excited state aromatic in S_1 having a more C–C bond length equalised perimeter and a short transannular C–C bond in the pentalene moiety (cf., two allylic fragments with an ethylene fragment in between). This is principally the same effect that led to the large Stokes shift of 1.50 eV (12 300 cm^{-1}) observed experimentally by Wan and Shukla for dibenzooxepins,[38] another benzannelated 8π-electron cycle. The relaxation energy in S_1 for pentalene derivatives varies with the computational method and is found to be in the range 0.6–0.9 eV using CASPT2 and ~1.0 eV using SF-TD-DFT (Table S6).

Noteworthily, the SF-TD-DFT geometry optimisations to the adiabatic S_1 states lead to states that, for some of the molecules, are mixtures of all states considered (S_0, S_1, and T_1) with near-degenerate energy levels and high spin contamination. Although difficult to interpret, these results indicate that the S_1 state tends toward a state mixing with S_0 (cf., conical intersection, vide infra), which experimentally would lead to a fast radiationless decay to S_0. Such a process will severely hamper the use of pentalene derivatives as SF chromophores as their non-radiative decay likely outcompetes any SF process, similar to what has been concluded for other SF chromophore candidates.[70]

The SF-TD-DFT results further show that the adiabatic energies $E(S_{1a})$ of the molecules explored lead to $E(S_{1a})/E(T_{1a})$ ratios in the range 0.9–1.6 for non-**BORAZA** compounds and 1.20–1.90 for **BORAZA** compounds (Table S2). For most of the compounds, this is much lower than the corresponding ratios of known SF chromophores (e.g., for tetracene it is 1.86 based on experimental energies[10] and 1.79 based on computed $E(S_{1a})$ and $E(T_{1a})$). Notably, some of the compounds with the highest $E(S_{1v})/E(T_{1a})$ ratios according to the ZHA approach have the lowest $E(S_{1a})/E(T_{1a})$ ratios, and some even have inverted S_1–T_1 gaps, whereby $E(S_1)/E(T_1) < 1$ (Fig. S48). The latter is, in itself, not surprising given that the parent pentalene is a known inverted singlet–triplet gap molecule, for which the relaxation from the vertically excited C_{2h} symmetric S_0 geometry to the optimal D_{2h} symmetric geometries of the S_1 and T_1 states flips the energy order between the two excited states.[16] As **MBP** follows the same changes in the orbital configuration as pentalene when going from S_0 to T_1, it is obvious that our computed $E(S_{1v})/E(T_{1a})$ ratios of benzannelated pentalenes are exaggerated as one must take into consideration large relaxation energies in S_1. Accordingly, these compounds cannot function as SF chromophores. Likely, the more a pentalene derivative's excited-state aromaticity resembles that of the parent pentalene, the more similar its excited-state PES features are. One can postulate that the feature of large relaxation energies in S_1 will occur in many compounds that are strongly Baird-aromatic in T_1 and S_1 and Hückel-antiaromatic in S_0. Hence, adiabatic S_1 energies should be used for proper estimation of the first SF energy criterion of such compounds.

As noted above, a few of the monobenzoborazapentalenes (**BORAZA4**, **BORAZA6**, **BORAZA8** and **BORAZA9**) satisfied the ZHA energy requirement (Table 1, entries 43, 45, 47, and 48). Yet again, when the ratios are based on the adiabatic S_1 energies, most of these compounds do not fulfil the first SF

energy criterion of $2 \leq E(S_1)/E(T_1)$ (Table S2). There are two exceptions, **BORAZA4** and **BORAZA8**, with ratios even slightly above that of tetracene (Table S2), and these may function as templates for designing heteropentalene-based SF chromophores. A drawback is that both these compounds have low T_1 state energies, which limit their practical applications.

At this point, one may ask if steric bulk can impact the $E(S_1)/E(T_1)$ ratios of the pentalene derivative. Four bulky t-Bu substituents freeze the bond-length alternate pentalene structure (Fig. 1) and hinder the pentalene core from adopting an approximate D_{2h} symmetry in the S_1 and T_1 states. This compound maintains the SF energy criterion according to the ZHA scheme, but when the $E(S_1)/E(T_1)$ ratio is based on the adiabatic energies, we found a ratio of 1.31, far from sufficient (Table S2). Moreover, the $f(S_0–S_1)$ value is zero for this compound.

Presence of S_1/S_0 conical intersections

Rapid non-radiative decay to the S_0 state via conical intersections (CIs) is a process that can compete with singlet fission, and both intramolecular and intermolecular factors (e.g., hydrogen-bonding) can open such decay channels.[70] Indeed, as noted above, a clear drawback of pentalene derivatives is the potential presence of CIs between the S_1 and S_0 states.[47]

To explore the presence of CIs, additional investigations of the optimal S_1 geometries that are affected by spin contamination in SF-TD-DFT were performed via CASSCF optimisations, with energies evaluated using CASPT2 (CASPT2/ANO-RCC-VTZP//CASSCF(12,12)/ANO-RCC-VTZP) (see the Methodology section for references). The results from these computations show a higher energy of the adiabatic S_1 state than when based on the SF-TD-DFT optimised states, with the weights of the S_1 and S_0 configurations showing a flip in energy ordering relative to each other. More explicitly, the electron configuration that corresponds to the S_0 state is in some compounds higher in energy than that of the S_1 state at the S_1 optimised geometry. This indicates an S_1–S_0 CI along the path that leads from the S_0 geometry to that of the S_1 state. Yet, this feature varies from molecule to molecule. **MBP** has the most apparent such feature, with the electron configuration for S_1 being lower in energy than the configuration for S_0 by 0.5 eV. In contrast, **AZA4** and **PYR3** have calculated CASPT2 excited states in close agreement with the states optimized with SF-TD-DFT (Table S3). Notably, the latter are also the compounds with no spin-contaminated states at the optimised S_1 geometry according to the SF-TD-DFT calculations, and they exhibit no reversal in the energy ordering of the S_0 and S_1 states (S_1 is about 0.4–0.5 eV higher than S_0). This indicates that **AZA4** and **PYR3** are able to avoid the CI, which suggests that it should be possible to design (hetero)pentalenes that do not decay from the S_1 state via a CI to the S_0 state. Of the two borazapentalenes with suitable $E(S_{1a})/E(T_{1a})$ ratios for SF, only **BORAZA8** has pure spin states, suggesting that its optimal S_1 geometry is located away from a CI between S_1 and S_0.

As observed above, four bulky substituents placed at 2-, 3-, 6-, and 7-positions can force the molecule in S_1 to maintain a bond length alternate structure with long C–C bonds between

6900 | Phys. Chem. Chem. Phys., 2026, **28**, 6894–6907

This journal is © the Owner Societies 2026

the C atoms with the bulky substituents as in S_0. However, the CI region is still available as it is primarily reached by shortening of the transannular C–C bond,[47] a bond that is unaffected by the bulky substituents. Indeed, as observed in the measurements on 1,3,5-tri(*tert*-butyl)pentalene, there are no signs of emission from the first excited state.[5] Emission is only visible from higher excited states. Clearly, a number of different aspects must be considered when designing chromophores for SF applications based on pentalene cores, whilst avoiding the CI relaxation pathway.[70]

Antiaromaticity in S_0 and aromaticity in T_1

Next, we assessed which molecules have reduced antiaromatic character in S_0, leading to increased thermal stability, and which molecules have Baird-aromatic character in T_1, leading to increased photostability. This analysis is based on various computed (anti)aromaticity indicators as described in the Computational tools section. In brief, the analysis is based on the geometric HOMA,[63,64] the magnetic NICS[57–59,61,62] and ACID,[55,56] and the electronic FLU[52–54] and MCI[51] (anti)aromaticity descriptors.

To facilitate comparison of the (anti)aromatic characters of differently large heteroareno- and bis(heteroareno)pentalenes, the geometric and electronic indices (HOMA, MCI and FLU) were evaluated at the 8π-electron ring of the pentalene moiety. For the magnetic descriptors, this may lead to differences in the assessment of the (anti)aromatic character as the magnetically induced diatropic (aromatic) ring currents in the T_1 states primarily involve the perimeters of the molecules (Fig. S1–S7 and S13–19). Still, there is no unambiguous way to determine the T_1 state Baird-aromaticity in the tricyclic class A compounds having both 8π- and 12π-electron cycles and the tetracyclic class D compounds (*vide infra*), which in addition have 16π-electron cycles. Any comparison of the (anti)aromatic characters of differently sized polycyclic molecules will necessarily be somewhat ambiguous.

With this uncertainty in the background, we compared the values of the descriptors against the correspondingly computed values of dibenzo[*a,e*]pentalene, which is persistent at ambient temperature,[27] thereby estimating the thermal stabilities of our pentalenes in their S_0 states. Yet, also steric bulk can stabilize the pentalene core as 1,3,5-tri(*tert*-butyl)pentalene is persistent.[26] As the FLU values of monoheteroarenopentalenes in classes A–C are higher than those of dibenzo[*a,e*]pentalene (Fig. S46), while the MCI and HOMA values in the pentalene unit are lower, our conclusion from this comparison is that they likely will need some steric protection to prevent dimerizations and other reactions in S_0.

The four pyridine derivatives **PYR1–PYR4** exhibited the most similar characteristics to **MBP**, with slightly alleviated S_0 Hückel-antiaromaticity in the pentalene core compared to the parent pentalene, while the Baird-aromaticity in T_1 is somewhat attenuated (Fig. 5A, S1, S13, S14, S38, and 39). As shown in Fig. S47, **MBP** and **PYR1–PYR4** in S_0 have lower MCI and HOMA values than those of the parent pentalene, while the FLU values are higher. In the T_1 state, the differences are the opposite. Yet, the S_0 antiaromatic and T_1 aromatic characters of the species

with fused 5-MR heteroaromatics (**FUR1–PYRO3**) depend heavily on the annelation pattern (Fig. 5A and Fig. S2, S3, S15–S17, S38, and S39). Clearly, annelation *via* the formal C–C single bond alleviates the S_0 antiaromatic character more extensively than annelation *via* the formal double bond of the heteroaromatic cycle (Fig. 5A), which is in line with previous results.[28] Thus, when evaluated through comparison with the S_0 antiaromatic character of the pentalene unit of dibenzo[*a,e*]pentalene, **FUR1–PYRO3** should be persistent at ambient temperature (Fig. S46). However, moving to the T_1 state, annelation at one of the formal C–C single bonds of pentalene resulted in less Baird-aromatic character in the pentalene unit than annelation at one of the double bonds according to all descriptors.

Interestingly, we observe a substantial correlation ($R^2 = 0.957$) between $E(T_1)$ and the (anti)aromaticity difference between the S_0 and T_1 states of compounds in class A as determined by MCI for the pentalene moiety (Fig. 5B). There are also significant correlations when the S_0–T_1 (anti)aromaticity differences are determined by either the electronic FLU ($R^2 = 0.845$) or the geometric HOMA ($R^2 = 0.863$) indices (Fig. 5C and D). These findings expand on our previous observations that, within classes of related monocyclic π-conjugated molecules, the energies of the lowest $\pi\pi^*$ states can be tuned by gains in excited state aromaticity.[12] However, such correlations are absent when sets of different classes of polycyclic $4n\pi$-electron compounds are compared.[43]

With a carbon-to-heteroatom replacement at the pentalene unit itself (class C), the effect on S_0 antiaromaticity and T_1 aromaticity depends on the type of atom inserted. The aza-substitutions in the parent (di- or tri-)azapentalenes and the benzannelated **AZA1–AZA4** and **DIAZA1–DIAZA6** generally lead to similar T_1 Baird-aromaticity of the 8π-electron (di)azapentalene unit when considering the MCI values as, respectively, pentalene and **MBP**. However, it is found from the NICS values and ACID plots that not all **DIAZA** derivatives are globally excited state aromatic because **DIAZA2**, **DIAZA4** and **DIAZA6** show signs of diatropic (aromatic) ring currents only on the ring furthest from the benzene moiety (Fig. S5, S20, and S21).

Also, the C_2-to-BN replacement in the pentalene moiety will, according to NICS scans, in most cases, destroy the global diatropic (aromatic) ring currents in the T_1 state (Fig. S7) when compared to **MBP**. Two exceptions are **BORAZA1** and **BORAZA8**, which retain global diatropic ring currents, and this is positive as **BORAZA8** also has a similar $E(S_{1a})/E(T_{1a})$ to that of tetracene (1.84 *vs.* 1.79, Table S2). With regard to the electronic and geometric (anti)aromaticity descriptors, the MCI and HOMA values for all class C **BORAZA** compounds in their T_1 states are negligible (Fig. 5A and S38, respectively), matching the nonaromatic character. Furthermore, when the B and N atoms are in different rings (**BORAZA5–BORAZA10**), the pentalene unit can often be separated into formal borole and pyrrole rings based on NICS scans (Fig. S7). This indicates that the C_2-to-BN replacement, despite leading to substantial $f(S_0–S_1)$ values (Table 1), is often a too large change considering our goal to design excited-state aromatic SF chromophores with accessible optical transitions. Moreover, as borole rings have substantial antiaromatic character in S_0,[8] these species are possibly not
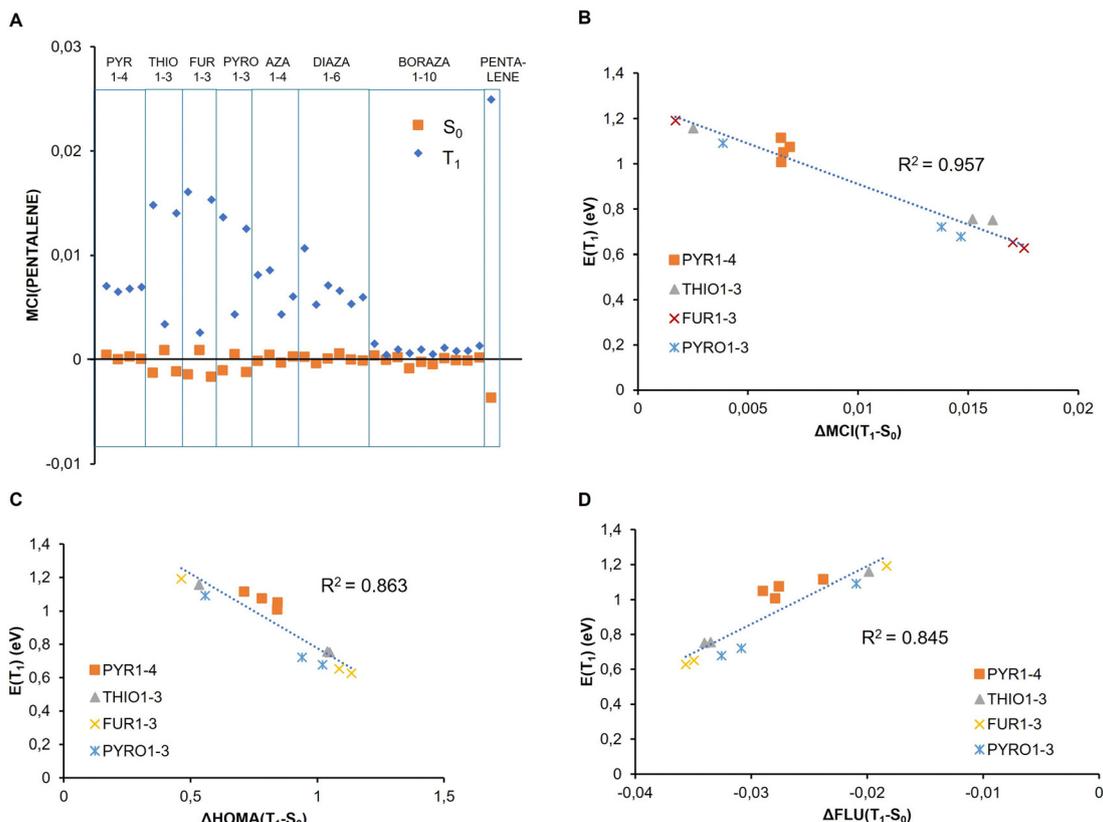
This journal is © the Owner Societies 2026

Phys. Chem. Chem. Phys., 2026, **28**, 6894–6907 | **6901**

Fig. 5 (A) MCI values of the pentalene unit in S_0 (orange squares) and T_1 (blue circles) for the compounds in class A and class C in Fig. 1. (B) Changes in the MCI of the pentalene moiety in the molecules of class A when going from S_0 to T_{1a} versus $E(T_1)$. A larger $\Delta MCI(T_1-S_0)$ indicates a larger gain in aromaticity upon excitation. (C) Changes in the HOMA of the pentalene moiety in the molecules of class A when going from S_0 to T_{1a} versus $E(T_1)$. A larger $\Delta HOMA(T_1-S_0)$ indicates a larger gain in aromaticity upon excitation. (D) Changes in the FLU of the pentalene moiety in the molecules of class A when moving from S_0 to T_{1a} versus $E(T_1)$. A gradually more negative $\Delta FLU(T_1-S_0)$ value indicates a gradually larger gain in aromaticity.

stable thermally. On the positive side, given their relatively high excitation energy and lack of globally (anti)aromatic character, it is likely that these compounds will not have an accessible S_1/S_0 CI, and, accordingly, not exhibit ultrafast relaxation to S_0. However, a severe drawback is that the adiabatic energies for the S_1 state lead to ratios that are much lower (most commonly $E(S_{1a})/E(T_{1a}) \approx 1.4$, except **BORAZA6** and **BORAZA9** having $E(S_{1a})/E(T_{1a}) \approx 1.6$, and **BORAZA4** and **BORAZA8** reaching $E(S_{1a})/E(T_{1a}) \approx 1.9$, Table S2) than those obtained using the ZAH approach. Thus, it is apparent that one must compute both adiabatic S_1 and T_1 energies for proper assessment of the $E(S_1)/E(T_1)$ ratios of SF chromophore candidates that are potentially Baird-aromatic in their lowest excited states.

Dependence of $f(S_0-S_1)$ on pentalene's S_0 antiaromaticity

In the Introduction section, we brought up a potential connection between lowered S_0 antiaromatic character in pentalene derivatives and an increase in $f(S_0-S_1)$. However, as shown in Fig. 6, there is in general no correlation between the antiaromatic character in S_0 and $f(S_0-S_1)$, neither when using an electronic (anti)aromaticity indicator (Fig. 6A) nor when using a magnetic one (Fig. 6B). Although there are nonaromatic pentalene derivatives with high $f(S_0-S_1)$, there are also those

with highly antiaromatic character in S_0 with high $f(S_0-S_1)$, as well as nonaromatic ones with low $f(S_0-S_1)$. This reveals that factors beyond the extent of antiaromatic character in S_0 influence the $f(S_0-S_1)$ value. Hence, the hypothesis that antiaromaticity alleviation in S_0 leads to increased oscillator strength is oversimplified.

Merging of findings for SF chromophore design

The best-performing C-to-heteroatom and -heteroarene annelations in classes A–C with regard to (i) high oscillator strength, (ii) markedly aromatic character in T_1 and S_1, and (iii) reduced antiaromatic character in S_0 were combined and tested. This leads to class D pentalenes composed of mono(heteroareno)borazapentalenes (Fig. 7A and B) and bis(heteroareno)pentalenes (Fig. 7C and D). To be beneficial, the pentalene derivatives should, in addition to features (i)–(iii), also have both SF energy criteria satisfied and low probabilities for nonradiative decay from S_1 to S_0 via conical intersections. The latter was estimated via SF-TD-DFT computations by investigating how spin-contaminated T_1, S_1 and S_0 states are at the S_1 geometry; we argue that those with spin-contaminated states have easy access to CIs. For the class D species, we discuss, in order, the $f(S_0-S_1)$ values, the $E(S_1)/E(T_1)$ ratios, and their S_0 antiaromatic and T_1 aromatic characters.
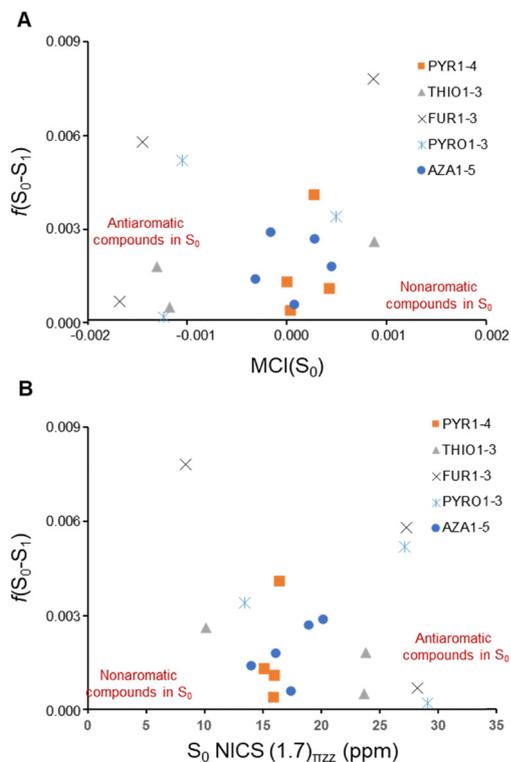
6902 | *Phys. Chem. Chem. Phys.*, 2026, **28**, 6894–6907

This journal is © the Owner Societies 2026

Fig. 6 (A) The oscillator strengths for the S_0–S_1 transition ($f(S_0$–$S_1)$) versus the MCI values of the pentalene unit in the pentalene derivatives of classes A and C in their S_0 states. (B) The oscillator strengths $f(S_0$–$S_1)$ versus the maximal NICS value for the heteroarenoannelated pentalenes of classes A and C in their S_0 states.

The calculated $f(S_0$–$S_1)$ values of class D pentalenes are in some cases significantly larger than that of **MBP**, by up to a factor of 90. Thus, they reach 67% of the value of pentacene. The most notable increases are observed when the modifications that lead to large $f(S_0$–$S_1)$ in classes A and C are combined. On the other hand, the $f(S_0$–$S_1)$ values are reduced for some of the mono(heteroareno)borazapentalenes when compared to the monobenzoborazapentalenes (*e.g.*, **BORAZA1**), as shown in Fig. 7A. For the **BORAZA8** derivatives, we observe increased oscillator strengths compared to the parent compound of the thiopheno and pyrrolo annelated ones, while furano derivatives have lower $f(S_0$–$S_1)$ values.

Moving to the bis(heteroareno)pentalenes, they have higher computed $f(S_1$–$S_0)$ than those of the mono(heteroareno)-pentalenes of classes A–C (Table 1 and Table S3). Particularly, unsymmetrical annelations of 1–$3'$ and 3–$1'$ types (Fig. 7B and 7C) lead to increased oscillator strengths. However, unsurprisingly, the symmetry achieved through the 3–$3'$ and 1–$1'$ annelation patterns leads to negligible $f(S_0$–$S_1)$ values. Here, the negligible $f(S_0$–$S_1)$ values of the 3–$3'$-**ZPYR** compounds (with Z = **FUR**, **PYRO** or **THIO**) may seem contradictory as the compounds are unsymmetric because of the size difference of the two annelated rings (one 5-MR and one 6-MR). Yet, as 3–$3'$ annelation leads to similar distortions of the HOMO and the LUMO, they are localized at the same parts of the molecule, while 1–$3'$ annelations lead to distortive effects in different

directions, leading to increased $f(S_0$–$S_1)$ irrespective of the ring size.

Regarding the $2 \leq E(S_1)/E(T_1)$ criterion, none of the mono-(heteroareno)boraza-pentalenes based on **BORAZA1** annelated at the 2-position (Fig. 7A) satisfy this criterion according to the ZHA approach due to the high energy of the S_1 and T_1 states (Table S3). This leads to low $E(S_{1v})/E(T_{1a})$ ratios (Table S3) and indicates that these substitution patterns are worse than those of compounds in classes A and C. Conversely, annelations at the 1- and 3-positions lead to fulfilment of the SF energy criterion according to the ZHA approach. Yet, the increase in $f(S_0$–$S_1)$ for these annelation patterns is negligible when compared to their non-**BORAZA** equivalents. However, all of the heteroannelated **BORAZA8** derivatives satisfy the energetic criteria for SF according to the ZHA approach, and those annelated at the 1- and 3-positions also satisfy them, as calculated using adiabatic S_1 energies (Table S5). This suggests that the **BORAZA8** derivatives are suitable candidates for future synthetic efforts, although $E(T_1)$ is slightly too small for silicon-based SF chromophores.

The bis(heteroareno)pentalenes **FURPYR**, **FURTHIO** and **PYROTHIO** barely maintain the ZHA scheme SF criterion (see Table S3), and their $E(T_1)$ values are mostly low (approximately 0.6–0.8 eV). Hence, they are below what is applicable together with today's crystalline silicon (c-Si) solar cells. The exceptions are the two **FURPYR** species with calculated $E(T_1)$ values in the range of 1.05–1.08 eV. However, when the adiabatic ratios are calculated, the SF criterion is far from satisfied because all bis(heteroareno)pentalenes have $E(S_{1a})/E(T_{1a})$ ratios in the range 1.1–1.4 (Fig. S51). Furthermore, these compounds show spin-contaminated S_0, S_1, and T_1 states with SF-TD-DFT optimisation of S_1. This entails a nearby conical intersection and casts doubt on the validity of the calculated adiabatic S_1 energies. The expectations are the **ZPYR** compounds, which show no spin-contaminated states.

The compounds in class D are all less S_0 antiaromatic than **MBP**, in line with what applies to dibenzo[a,e]pentalene. With regard to the (anti)aromatic character of the **ZBORAZA** compounds, they are nonaromatic in both S_0 and T_1 based on MCI (Fig. 7D), with variations in the degree of aromaticity based on the (anti)aromaticity index considered. Indices like NICS (Fig. S9) and HOMA (Fig. S44) show diminished excited-state aromatic character for the **ZBORAZA** compounds. Such low excited state aromatic character casts doubt on the suitability of the borazapentalenes as chromophores for SF applications as they may not exhibit sufficient photostability. In contrast, the bis(heteroareno)pentalenes in their T_1 states maintain (diminished) Baird-aromatic characters in the pentalene cores when analysed using various (anti)aromaticity descriptors (Fig. 7E and F, Fig. S8, S10–12, and S29–37). Conversely, two one-bond to one-bond annelations in the form of the 2–$2'$ annelation (Fig. S52) render the molecules nonaromatic in S_0, and also not Baird-aromatic in T_1. Similar results were observed for the 2–$1'$ and 2–$3'$ annelation patterns and as such were not investigated.

Taken together, the bis(heteroareno)pentalenes show increased $f(S_0$–$S_1)$ values, although the oscillator strengths are
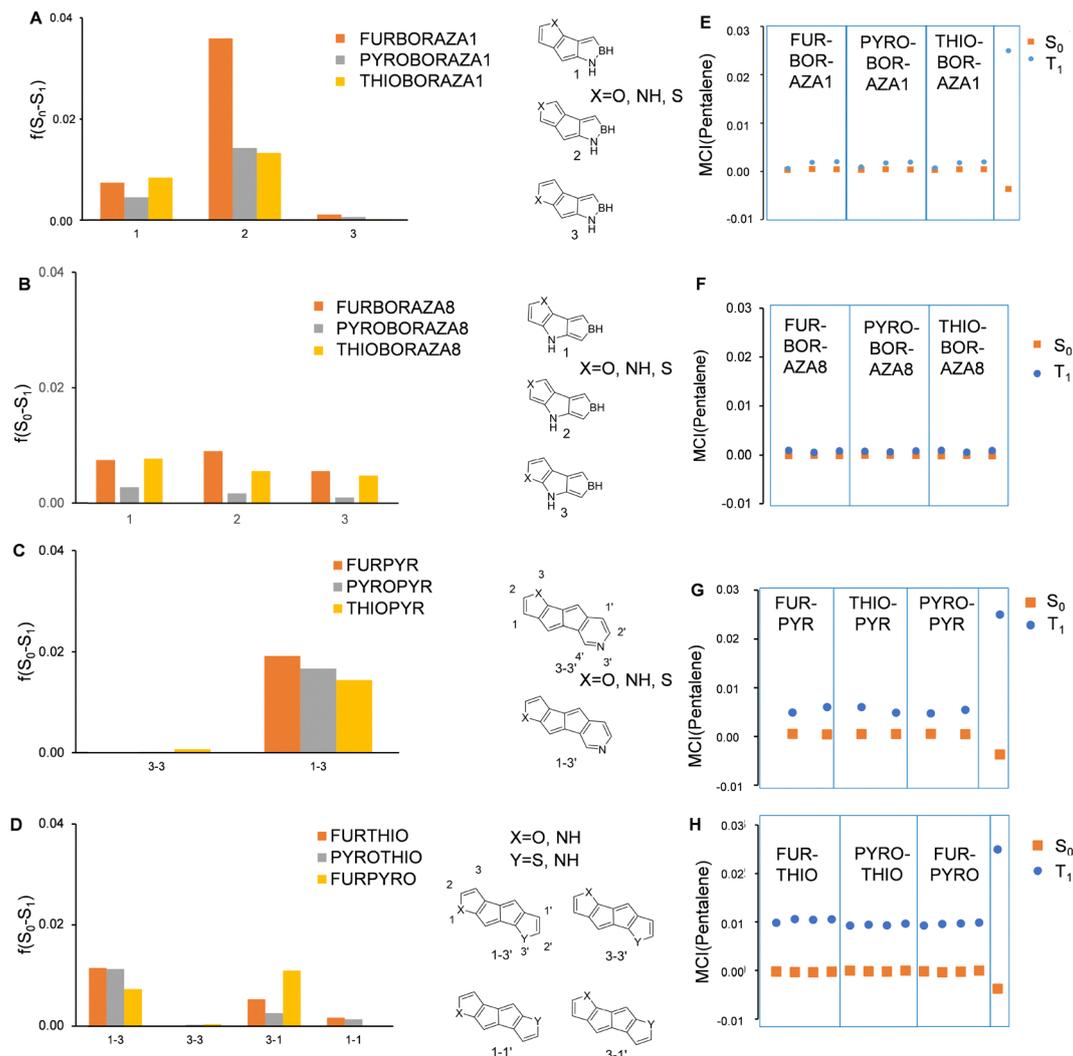
This journal is © the Owner Societies 2026

Phys. Chem. Chem. Phys., 2026, **28**, 6894–6907 | **6903**

Fig. 7   Pentalene derivatives with annelations that lead to increased oscillator strength f (S_0–S_1). (A) Borazapentalenes based on the **BORAZA1** derivative, fused with 5-MR heteroarenes, (B) borazapentalenes based on the **BORAZA8** derivative, fused with 5-MR heteroarenes, (C) bis(heteroareno)pentalenes (the nomenclature is shown in the figure), with pyridine as the other heteroareno compound, and (D) bis(heteroareno)pentalenes. X in the first part of the compound name signifies O (labelled **FUR**) or NH (labelled **PYRO**), while Y signifies S (labelled **THIO**) or NH (labelled **PYRO**) as the corresponding annelation in the second part of the compound label. (E) MCI values of the pentalene unit for the compounds in panel (A). (F) MCI values of the pentalene unit for the compounds in panel (B). (G) MCI values of the pentalene unit for the compounds in panel (C). (H) MCI values of the pentalene unit for the compounds in panel (D).

still rather modest. Moreover, they maintain some Baird-aromatic character in their T_1 states, but given that the adiabatic ratios are significantly below 2 (in the range of 1.2–1.4), this indicates that these compounds are unsuitable as SF chromophores.

Conclusions and outlook

To conclude, heteroatomic analogues of mono- and dibenzo-pentalenes were studied in order to find a way to overcome the symmetry-forbidden nature of the S_0–S_1 transition, which can benefit future applications in singlet fission photovoltaics. By introducing heteroatoms and thereby lowering the symmetry of the compounds, the distribution of the frontier molecular orbitals is changed, and accordingly, the oscillator strengths

of the S_0–S_1 transitions were increased. At best, a computed oscillator strength of this transition which is two thirds that of pentacene, a well-established SF chromophore, is achieved. Overall, we reveal the possibility of carbon-to-heteroatom replacements to increase the allowedness of the transition to the first singlet excited state of pentalene-based chromophores. One may postulate that substituents can be used to tailor this feature further. Substituents will likely also be needed to stabilize the mono(heteroareno)heteropentalenes, while the bis(heteroareno)heteropentalenes could be stable at ambient temperatures based on the comparison of their S_0 antiaromatic characters with those of pentalene, monobenzopentalene and dibenzo[a,e]pentalene.

However, their potential in singlet fission photovoltaic applications for increased solar cell efficiency is diminished

due to their significant geometric relaxation after excitation to the S_1 state. Only a very small number of heteropentalenes (one class of heteroarenoborazapentalenes) were identified with $E(S_1)/E(T_1)$ ratios that resemble that of tetracene when fully based on adiabatic energies. This, in conjunction with both the modest to moderate oscillator strengths compared to other chromophores, and the presence of accessible conical intersections leading from S_1 to S_0 and rapid non-radiative decay, is not promising. Thus, the prospect of using pentalene-based molecules as SF chromophores is rather bleak. Although this is a negative finding, it can pave the way to other related compound classes with more suitable properties to function as SF chromophores. The pentalene derivatives explored here may instead be useful for other optoelectronic applications.

On the general side, we find that computational screening of potential SF chromophores that can be Baird-aromatic in their S_1 and T_1 states must be based on both adiabatic S_1 and T_1 energies. Through our study, we thereby pinpoint a severe drawback of molecules that are strongly Hückel-antiaromatic in S_0 and strongly Baird-aromatic in T_1 and S_1 because the large relaxation energy in S_1 renders them unsuitable as singlet fission chromophores. More modest antiaromatic character in S_0 and aromatic character in S_1 and T_1 should be desirable if they are to function in singlet fission photovoltaics.

Computational methodology

Geometry optimisations in the S_0 and T_1 states were performed with Gaussian 16[71] using the (U)M06-2X hybrid functional with the def2-TZVPD basis set,[72,73] and the observation of vibrational frequencies shows these structures as minima. TD-DFT calculations were performed on the optimised S_0 structures to obtain vertical excitation energies, and the optimised ground state structures were used as initial guesses for the T_1 geometry optimisations. Geometry optimisations of adiabatic S_1 states (S_{1a}) were performed with SF-TD-DFT using the ORCA software,[74–78] employing the M06-2X hybrid functional and the def2-TZVPD basis set.[72,73] The results obtained using the M06-2X functional were compared with those obtained using the BHHLYP functional and were found to be comparable. Geometry optimization with CASSCF at the CASSCF(12,12)/ ANO-RCC-VTZP level was performed with implementation in the OpenMolcas software[79–83] and further evaluated at the single point CASPT2/ANO-RCC-VTZP level.

Aromaticity was assessed using the geometric harmonic oscillator model of aromaticity (HOMA)[63,64] index, the magnetic nucleus independent chemical shift (NICS)[57–62] and anisotropy of induced current density (ACID)[55,56] descriptors, and the electronic fluctuation (FLU)[52–54] and multicenter (MCI)[51] indices to assess the degree of (anti)aromaticity. Computations of NICS were carried out using the NICS-XY scan methods with $NICS(1.7)_{\pi zz}$ in which NICS values are probed along a path at a distance of 1.7 Å above the molecular plane. The HOMA values were calculated based on the definition. The $NICS(r)_{\pi zz}$ values were generated using the Aroma package, which can generate

the saturated structures to separate the σ-skeleton's contribution. In the excited state calculations, we used the ground state contribution of the σ-skeleton. ACID plots were generated using the AICD program,[56] and MCI and FLU computed using the EDI-3D program package.[54] These aromaticity analyses were carried out at the M06-2X/def2-TZVP level.

Conflicts of interest

There are no conflicts to declare.

Data availability

The data underlying this study are openly available in the published article and its supplementary information (SI). The data supporting this article have been included as part of the SI. Supplementary information: Section S1: Computed excitation parameters; Section S2: NICS scans; Section S3: ACID plots; Section S4: Plots of MCI and FLU; and HOMA values of the pentalene unit; Section S5: Miscellaneous; Section S6: Conical intersection in MBP; Section 7: Supplementary references; and Section S8: Cartesian coordinates and absolute energies for all calculated structures. See DOI: https://doi.org/10.1039/d5cp04492h.

Acknowledgements

References

1 H. Hopf, *Angew. Chem., Int. Ed.*, 2013, **52**, 12224–12226.
2 F. Neumann and K. Jug, *J. Phys. Chem.*, 1995, **99**, 5834–5837.
3 T. Bally, S. Chai, M. Neuenschwander and Z. Zhu, *J. Am. Chem. Soc.*, 1997, **119**, 1869–1875.
4 J. Zhu, K. An and P. v R. Schleyer, *Org. Lett.*, 2013, **15**, 2442–2445.
5 L. Bussotti, P. Foggi, C. Gellini, L. Moroni and P. R. Salvi, *Phys. Chem. Chem. Phys.*, 2021, **3**, 3027–3033.
6 S. Jalife, A. Tsybizova, R. Gershoni-Poranne and J. I. Wu, *Org. Lett.*, 2024, **26**, 1293–1298.
7 D. Xing, F. Glöcklhofer and F. Plasser, *Chem. Sci.*, 2024, **15**, 17918–17926.
8 C. Hong, J. Baltazar and J. D. Tovar, *Eur. J. Org. Chem.*, 2022, e202101343.

This journal is © the Owner Societies 2026

Phys. Chem. Chem. Phys., 2026, **28**, 6894–6907 | **6905**

9 T. Kawase, T. Fujiwara, C. Kitamura, A. Konishi, Y. Hirao, K. Matsumoto, T. K. H. Kurata, S. Shinamura, H. Mori, E. Miyazaki and K. Takimiya, *Angew. Chem., Int. Ed.*, 2010, **49**, 7728–7732.

10 M. B. Smith and J. Michl, *Chem. Rev.*, 2010, **110**, 6891–6936.

11 M. C. Hanna and A. J. Nozik, *J. Appl. Phys.*, 2006, **100**, 074510.

12 O. E. Bakouri, J. R. Smith and H. Ottosson, *J. Am. Chem. Soc.*, 2020, **142**, 5602–5617.

13 J. Usuba, M. Hayakawa, S. Yamaguchi and A. Fukazawa, *Chem. – Eur. J.*, 2021, **27**, 1638–1647.

14 T. Gazdag, P. J. Mayer, P. P. Kalapos, T. Holczbauer, O. E. Bakouri and G. London, *ACS Omega*, 2022, **7**, 8336–8349.

15 Ö. H. Omar, X. Xie, A. Troisi and D. Padula, *J. Am. Chem. Soc.*, 2023, **145**, 19790–19799.

16 M. H. Garner, J. T. Blaskovits and C. Corminboeuf, *Chem. Sci.*, 2023, **14**, 10458–10466.

17 J. Usuba and A. Fukazawa, *Chem. – Eur. J.*, 2021, **27**, 16127.

18 E. Meiszter, T. Gazdag, P. J. Mayer, A. Kunfi, T. Holczbauer, M. Sulyok-Eiler and G. London, *J. Org. Chem.*, 2024, **89**, 5941–5951.

19 L. Qiu, X. Zhuang, N. Zhao, X. Wang, Z. An, Z. Lan and X. Wan, *Chem. Commun.*, 2014, **50**, 3324–3327.

20 C. S. Anstöter and P. W. Fowler, *Chem. Phys. Chem.*, 2025, **26**, e202401069.

21 F. Fratev, V. Monev and R. Janoschek, *Tetrahedron*, 1982, **38**, 2929–2932.

22 P. Wan and E. Krogh, *J. Chem. Soc., Chem. Commun.*, 1985, **656**, 1207–1208.

23 R. Ayub, O. E. Bakouri, K. Jorner, M. Solà and H. Ottosson, *J. Org. Chem.*, 2017, **82**, 6327–6340.

24 M. Ueda, K. Jorner, Y. M. Sung, T. Mori, Q. Xiao, D. Kim, H. Ottosson, T. Aida and Y. Itoh, *Nat. Commun.*, 2017, **8**, 346.

25 J. Yan, T. Slanina, J. Bergman and H. Ottosson, *Chem. – Eur. J.*, 2023, **29**, e202203748.

26 A. Falchi, C. Gellini, P. Remigio Salvi and K. Hafner, *J. Phys. Chem.*, 1995, **99**, 14659–14666.

27 T. Kawase, A. Konishi, Y. Hirao, K. Matsumoto, H. Kurata and T. Kubo, *Chem. – Eur. J.*, 2009, **15**, 2653–2661.

28 C. K. Frederickson, L. N. Zakharov and M. M. Haley, *J. Am. Chem. Soc.*, 2016, **138**, 16827–16838.

29 T. Ullrich, D. Munz and D. M. Guldi, *Chem. Soc. Rev.*, 2021, **50**, 3485–3518.

30 Y. Wu, Y. Wang, J. Chen, G. Zhang, J. Yao, D. Zhang and H. Fu, *Angew. Chem., Int. Ed.*, 2017, **56**, 9400–9404.

31 N. C. Baird, *J. Am. Chem. Soc.*, 1972, **94**, 4941–4948.

32 M. Rosenberg, C. Dahlstrand, K. Kilså and H. Ottosson, *Chem. Rev.*, 2014, **114**, 5379–5425.

33 M. Solà, *Nat. Chem.*, 2022, **14**, 585–590.

34 M. Solà, *Wiley Interdiscip. Rev. Comput. Mol. Sci.*, 2019, **9**, e1404.

35 J. Aihara, *Bull. Chem. Soc. Jpn.*, 2016, **89**, 1425–1454.

36 F. Feixas, E. Matito, J. Poater and M. Solà, *Chem. Soc. Rev.*, 2015, **44**, 6434–6451.

37 R. Kotani, L. Liu, P. Kumar, H. Kuramochi, T. Tahara, P. Liu, A. Osuka, P. B. Karadakov and S. Saito, *J. Am. Chem. Soc.*, 2020, **142**, 14985–14992.

38 D. Shukla and P. Wan, *J. Am. Chem. Soc.*, 1993, **115**, 2990–2991.

39 K. Jorner, R. Emanuelsson, C. Dahlstrand, H. Tong, A. Denisova and H. Ottosson, *Chem. – Eur. J.*, 2014, **20**, 9295–9303.

40 S. Yadav, O. El Bakouri, K. Jorner, H. Tong, C. Dahlstrand, M. Solà and H. Ottosson, *Chem. – Asian J.*, 2019, **14**, 1870–1878.

41 M. Saunders, R. Berger, R. Breslow, J. M. H. Jr., C. Perchonock, E. Wasserman, R. S. Hutton and V. J. Kuck, *J. Am. Chem. Soc.*, 1973, **95**, 3017–3018.

42 R. Breslow, R. Hill and E. Wasserman, *J. Am. Chem. Soc.*, 1964, **86**, 5349–5350.

43 O. E. Bakouri, M. A. Johnson, J. R. Smith, A. K. Pati, M. I. Martin, S. C. Blanchard and H. Ottosson, *Chem. Sci.*, 2025, **16**, 7989–8001.

44 R. Casillas, I. Papadopoulos, T. Ullrich, D. Thiel, A. Kunzmann and D. M. Guldi, *Energy Environ. Sci.*, 2020, **13**, 2741–2804.

45 T. Gazdag, E. Meiszter, P. J. Mayer, T. Holczbauer, H. Ottosson, A. B. Maurer, M. Abrahamsson and G. London, *ChemPhysChem*, 2024, **25**, e202300737.

46 J. Zheng, X. Zhuang, L. Qiu, Y. Xie, X. Wan and Z. Lan, *J. Phys. Chem. A*, 2015, **119**, 3762–3769.

47 M. Bearpark, B. F. Bernardi, M. Olivucci and M. Robb, *Int. J. Quantum Chem.*, 1996, **60**, 505–512.

48 J. Wirz, in *Excited States in Organic Chemistry and Biochemistry. The Jerusalem Symposia on Quantum Chemistry and Biochemistry*, ed. B. Pullman and N. Goldblum, Springer, 1977, vol. 10, pp. 283–294.

49 D. Casanova and A. I. Krylov, *Phys. Chem. Chem. Phys.*, 2020, **22**, 4326–4342.

50 For an introduction on aromaticity and antiaromaticity see, M. Solà, A. I. Boldyrev, M. K. Cyrañski, T. M. Krygovski and G. Merino, *Aromaticity and Antiaromaticity: Concepts and Applications*, Wiley-VCH, New York, 2022.

51 P. Bultinck, R. Ponec and S. Van Damme, *J. Phys. Org. Chem.*, 2005, **18**, 706–718.

52 E. Matito, M. Duran and M. Solà, *J. Chem. Phys.*, 2005, **122**, 014109.

53 K. Jorner, F. Feixas, R. Ayub, R. Lindh, M. Solà and H. Ottosson, *Chem. – Eur. J.*, 2016, **22**, 2793–2800.

54 "ESI-3D program:" [Online]. Available at: https://quantchemdev.github.io/resources.html.

55 D. Geuenich, K. Hess, F. Köhler and R. Herges, *Chem. Rev.*, 2005, **105**, 3758–3772.

56 "AICD program package:" [Online]. Available at: https://www.otto-diels-institut.de/herges/pages_en/projects_acid.html.

57 R. Gershoni-Poranne and A. Stanger, *Chem. – Eur. J.*, 2014, **20**, 5673–5688.

58 A. Stanger, *J. Org. Chem.*, 2010, **75**, 2281–2288.

59 P. v R. Schleyer, C. Maerker, A. Dransfeld, H. Jiao and N. J. R. v E. Hommes, *J. Am. Chem. Soc.*, 1996, **118**, 6317–6318.

60 Z. Chen, C. S. Wannere, R. P. C. Corminboeuf and P. v R. Schleyer, *Chem. Rev.*, 2005, **105**, 3842–3888.

61 R. Gershoni-Poranne and A. Stanger, in *Aromaticity: Modern Computational Methods Applications*, ed. I. Fernández, Elsevier, 2021, p. 4.

6906 | *Phys. Chem. Chem. Phys.*, 2026, **28**, 6894–6907

This journal is © the Owner Societies 2026

62 A. Stanger and A. Rahalkar, "Aroma," [Online]. Available at: https://chemistry.technion.ac.il/en/team/amnon-stanger.

63 J. Kruszewski and T. M. Krygowski, *Tetrahedron Lett.*, 1972, **13**, 3839–3842.

64 T. M. Krygowski, H. Szatylowicz, O. A. Stasyuk, J. Dominikowska and M. Palusiak, *Chem. Rev.*, 2014, **114**, 6383–6422.

65 P. Mayer and H. Ottosson, *J. Phys. Org. Chem.*, 2025, **38**, e70000.

66 J. Michl and E. Thulstrup, *Tetrahedron*, 1976, **32**, 205–209.

67 C. G. Newton and C. A. Ramsden, *Tetrahedron*, 1982, **38**, 2965–3011.

68 P. Preethalayam, N. P. Vedin, S. Radenković and H. Ottosson, *J. Phys. Org. Chem.*, 2023, **36**, e4455.

69 T. Zeng, R. Hoffmann and N. Ananth, *J. Am. Chem. Soc.*, 2014, **136**, 5755–5764.

70 D. Z. Hook, R. Kilbride, D. J. Gillard, S. M. Rivero, R. K. Venkatraman, J. P. Pidgeon, A. Tartakovskii and J. Clark, *J. Mater. Chem. C*, 2025, **13**, 16981–16997.

71 M. J. Frisch, G. W. Trucks, H. B. Schlegel, G. E. Scuseria, M. A. Robb, J. R. Cheeseman, G. Scalmani, V. Barone, G. A. Petersson, H. Nakatsuji, X. Li, M. Caricato, A. V. Marenich, J. Bloino, B. G. Janesko, R. Gomperts, B. Mennucci, H. P. Hratchian, *et al.*, *Gaussian 16.*, Wallingford CT, 2016.

72 Y. Zhao and D. G. Truhlar, *Theor. Chem. Acc.*, 2008, **120**, 215–241.

73 F. Weigend, *Phys. Chem. Chem. Phys.*, 2006, **8**, 1057–1065.

74 F. Neese, Software update: the ORCA program system, version 5.0, *Wiley Interdiscip. Rev. Comput. Mol. Sci.*, 2022, **12**, e1606.

75 F. Neese and G. Olbrich, *Chem. Phys. Lett.*, 2002, **362**, 170–178.

76 F. Neese, *J. Comput. Chem.*, 2003, **24**, 1740–1747.

77 F. Neese, F. Wennmohs, A. Hansen and U. Becker, *Chem. Phys.*, 2009, **356**, 98–109.

78 F. Neese, The SHARK Integral Generation and Digestion System, *J. Comput. Chem.*, 2022, **44**, 381–396.

79 G. Li Manni, I. Fdez Galván, A. Alavi, F. Aleotti, F. Aquilante, J. Autschbach, D. Avagliano, A. Baiardi, J. J. Bao, S. Battaglia, L. Birnoschi, A. Blanco-González, S. I. Bokarev, R. Broer, R. Cacciari, P. B. Calio, R. K. Carlson, R. Carvalho Couto, L. Cerdán, L. F. Chibotaru, N. F. Chilton, J. R. Church, I. Conti, S. Coriani, J. Cuéllar-Zuquin, R. E. Daoud, N. Dattani, P. Decleva, C. de Graaf, M. G. Delcey, L. De Vico, W. Dobrautz, S. S. Dong, R. Feng, N. Ferré, M. Filatov(Gulak), L. Gagliardi, M. Garavelli, L. González, Y. Guan, M. Guo, M. R. Hennefarth, M. R. Hermes, C. E. Hoyer, M. Huix-Rotllant, V. K. Jaiswal, A. Kaiser, D. S. Kaliakin, M. Khamesian, D. S. King, V. Kochetov, M. Krośnicki, A. A. Kumaar, E. D. Larsson, S. Lehtola, M.-B. Lepetit, H. Lischka, P. López Ríos, M. Lundberg, D. Ma, S. Mai, P. Marquetand, I. C. D. Merritt, F. Montorsi, M. Mörchen, A. Nenov, V. H. A. Nguyen, Y. Nishimoto, M. S. Oakley, M. Olivucci, M. Oppel, D. Padula, R. Pandharkar, Q. M. Phung, F. Plasser, G. Raggi, E. Rebolini, M. Reiher, I. Rivalta, D. Roca-Sanjuán, T. Romig, A. A. Safari, A. Sánchez-Mansilla, A. M. Sand, I. Schapiro, T. R. Scott, J. Segarra-Martí, F. Segatta, D.-C. Sergentu, P. Sharma, R. Shepard, Y. Shu, J. K. Staab, T. P. Straatsma, L. K. Sørensen, B. N. C. Tenorio, D. G. Truhlar, L. Ungur, M. Vacher, V. Veryazov, T. A. Voß, O. Weser, D. Wu, X. Yang, D. Yarkony, C. Zhou, J. P. Zobel and R. Lindh, OpenMolcas v23.02, *J. Chem. Theory Comput.*, 2023, **19**, 6933–6991.

80 F. Aquilante, J. Autschbach, R. K. Carlson, L. F. Chibotaru, M. G. Delcey, L. De Vico, I. Fdez. Galván, N. Ferré, L. M. Frutos, L. Gagliardi, M. Garavelli, A. Giussani, C. E. Hoyer, G. Li Manni, H. Lischka, D. Ma, P. Å. Malmqvist, T. Müller, A. Nenov, M. Olivucci, T. B. Pedersen, D. Peng, F. Plasser, B. Pritchard, M. Reiher, I. Rivalta, I. Schapiro, J. Segarra-Martí, M. Stenrup, D. G. Truhlar, L. Ungur, A. Valentini, S. Vancoillie, V. Veryazov, V. P. Vysotskiy, O. Weingart, F. Zapata and R. Lindh, Molcas 8, *J. Comput. Chem.*, 2016, **37**, 506–541.

81 F. Aquilante, T. B. Pedersen, V. Veryazov and R. Lindh, *Wiley Interdiscip. Rev.: Comput. Mol. Sci.*, 2013, **3**, 143–149.

82 V. Veryazov, P. Widmark, L. Serrano-Andrés, R. Lindh and B. O. Roos, *Int. J. Quantum Chem.*, 2004, **100**, 626–635.

83 B. Helmich-Paris, B. d Souza, F. Neese and R. Izsák, *J. Chem. Phys.*, 2021, **155**, 104109.

This journal is © the Owner Societies 2026

Phys. Chem. Chem. Phys., 2026, **28**, 6894–6907 | **6907**